Article ID: 1000-324X(2023)06-0708-09 **DOI:** 10.15541/jim20220742

Photothermal Core-Shell TiN@Borosilicate Bioglass Nanoparticles: and Mineralization

WU Rui[1], ZHANG Minhui[1], JIN Chenyun[1], LIN Jian[1,2], WANG Deping[1,2]

(1. School of Materials Science and Engineering, Tongji University, Shanghai 201804, China; 2. Key Laboratory of Advanced Civil Engineering Materials, Ministry of Education, Tongji University, Shanghai 200092, China)

Abstract: Borosilicate bioglass has attracted extensive attention due to its stable structure and excellent biological activity. However, the rate of its mineralization process is fast in the initial stage and slow in the middle and late stages, which limits the application of borosilicate bioglass. As an auxiliary method, the near-infrared (NIR) laser can accelerate the degradation of bioglass. Therefore, we prepared a core-shell borosilicate bioglass with titanium nitride as the core and bioglass ($40SiO_2$-$20B_2O_3$-36CaO-$4P_2O_5$) as the shell, and used near-infrared laser regulation technology to intervene the mineralization process of the composite bioglass. The experimental results show that the core-shell bioglass exhibits a significant photothermal effect, and the photothermal ability increases with the increases of the doping amount of TiN NPs and the laser power density. During the *in vitro* immersion, near-infrared laser increased the degradation rate of bioglass. After immersion for 7 d, the contents of calcium and boron in the SBF are increased by 12%–16% and 8%–11%, respectively. Meanwhile, the formation efficiency of hydroxyapatite is significantly improved. Cell proliferation activity test shows that the sample has good biological safety. Therefore, near-infrared light can accelerate the degradation and mineralization of functional core-shell bioactive glass, which is expected to play a regulatory role.

Key words: borosilicate bioactive glass; core-shell structure; photothermal performance; mineralization

With the increasing global population and life expectancy, the number of patients with osteoporosis is growing rapidly and taking a high proportion. To make matters worse, with the aggravation of aging, osteoporosis and other bone diseases have become an important problem[1-2]. Common fracture treatment methods such as reduction and fixation, have poor prognoses for elderly patients and are prone to other complications[3]. The bioactive glass bone cement, with bioglass as the solid phase and natural polymer as the liquid phase, is an excellent material with good biodegradability and bone repair performance in clinical practice[4-6]. As a kind of bone-repairing biomaterial, borosilicate bioglass has attracted extensive attention due to its stable structure, excellent bioactivity, and bone conductivity. Hydroxyapatite is needed for human bone growth in the biochemical environment *in vivo*, and it can be formed on the surface of borosilicate bioglass. The release of boron ions can promote the proliferation of bone cells, calcium ions are adsorbed in the silicon-rich layer to construct bone-like hydroxyapatite crystals, which inhibits the bone absorption of osteoclasts, and shows good bone repair performance[7].

However, the conversion rate of bioglass in the mineralization process is uncontrollable. The degradation rate is fast at the initial stage but slow at the middle and late stages after implantation[8], which affects the curative effect at the middle and late stages and limits the application of borosilicate bioglass.

Photothermal therapy (PTT) is a common adjuvant therapy for bone tumor surgery[9-10]. The heat generated by PTT can not only kill tumor cells but also accelerate the degradation of ions in bioglass and improve the mineralization ability. Cao *et al*.[11] repaired the microcracks of the glass fiber composite containing Au NPs through the photothermal effect and improved the healing ability of the mineral trioxide aggregate (MTA) cement. Pinheiro *et al*.[12] used the photothermal effect to promote

Received date: 2022-12-06; **Revised date:** 2022-12-26; **Published online:** 2023-01-18
Foundation item: National Natural Science Foundation of China (51972232); National Key Research and Development Projects (2018YFC1106300)
Biography: WU Rui (1998–), female, Master candidate. E-mail: 2030621@tongji.edu.cn
吴 锐(1998–), 女, 硕士研究生. E-mail: 2030621@tongji.edu.cn
Corresponding author: LIN Jian, professor. E-mail: lin_jian@tongji.edu.cn
林 健, 教授. E-mail: lin_jian@tongji.edu.cn

the generation of hydroxyapatite phosphate of MTA in bone surgery *in vivo*, thereby improving the repair of complete tibial fractures treated by wire bone sutures. In addition, NIR laser has greater penetrability and less negative impact on human tissues, and 1064 nm wavelength is selected for NIR laser[13].

When choosing the photothermal agent doped with bioglass, it is necessary to consider the difficulty of the preparation process, photothermal performance, and biomedical activity *in vivo*. TiN NPs are a kind of excellent photothermal agents with stable performance and wide application, its strong photothermal stability and clinically recognized biosafety, and is used in cancer treatment and other aspects[14-15]. Yao *et al*.[16] prepared borosilicate glass composite bone cement doped with TiN NPs by mixed melting method, which provided an effective way to regulate the mineralization and ion release behavior of bioactive glass.

In addition, core-shell nano bioglass can further reduce the side effect of nuclear layer materials on cells, improve the uniformity of heat distribution of samples, and possess unique structural advantages[17-19]. Thus, the purpose of this study is to prepare core-shell composite bioactive glass by Sol-Gel method, with TiN NPs as the core and borosilicate bioglass as the shell, and to study photothermal effect, biological activity, ion release, and formation of mineralized products under 1064 nm NIR laser loading of the core-shell structure.

1　Materials and methods

1.1　Fabrication of core-shell nanoparticles

The core-shell structure was prepared by the Sol-Gel method[20]. As shown in Fig.1, 0, 0.02 and 0.04 g TiN NPs (50–100 nm, Hefei Zhonghang Nanometre Technology Development Co., Ltd) were respectively dispersed in ethanol through ultrasonic treatment. Deionized water and hexadecyl trimethyl ammonium bromide were added and stirred well. Tetraethyl orthosilicate (TEOS, AR), ammonia solution (28%(in mass), AR), tributyl borate (TBB, CP), triethyl phosphate (TEP, CP), and calcium nitrate tetrahydrate ($Ca(NO_3)_2{\cdot}4H_2O$, AR) were added successively, for reaction at 40 ℃ in a water bath for 3 h. Then the product was centrifuged and washed with water and ethanol for several times, and the obtained powder were dried and calcinated. Thereby, the core-shell particles with different contents of TiN NPs were obtained in which the core layer was TiN NPs and the shell layer was borosilicate bioglass composed of $40SiO_2$-$20B_2O_3$-$36CaO$-$4P_2O_5$(%, in mol), recorded respectively as *x*TiN@58S-20B (*x*=0.02, 0.04) while the sample without TiN NPs, recorded as 58S-20B, was used as control.

1.2　*In vitro* mineralization of the bioglass

The bioactivity of the material was tested through *in vitro* immersion test in simulated body fluid (SBF). 58S-20B, 0.02TiN@58S-20B, 0.04TiN@58S-20B were immersed in SBF at 37 ℃, as shown in Fig. 2(a), and 0.2 g bioglass samples were immersed in 20 mL SBF. To evaluate the influence of laser irradiation on the mineralization in a short time, the samples immersed in SBF were irradiated with 1 W/cm^2 NIR laser (1064 nm, 6 h/d) for up to 7 d, as shown in Fig. 2(b). The soaking solutions were taken out every day to detect pH change and phase composition of mineralized products.

1.3　Sample characterization

The surface morphology was examined using a field emission scanning electron microscope (FESEM, Hitachi S-4700) at 10 kV after being sputter-coated with gold, and a high-resolution field emission transmission electron microscope (TEM, JEM2100). The composition was analyzed by X-ray diffractometry (XRD, Smart Lab 9; Tokyo, Japan) using Cu Kα radiation (λ = 0.15406 nm) at a scanning rate of 10 (°)/min. The concentration of the ions released from bioglass into the SBF was tested by inductively coupled plasma atomic emission spectroscopy (ICP-AES, Optima 2100DV).

1.4　Proportion of TiN NPs

To obtain the proportion of TiN NPs of the core-shell structure, the sectional area and volume of the core and shell were calculated, respectively. According to the TEM image, we measured the approximate radii of the core layer and shell layer in the field of view, and calculated the cross-sectional areas of the core layer (S_c)

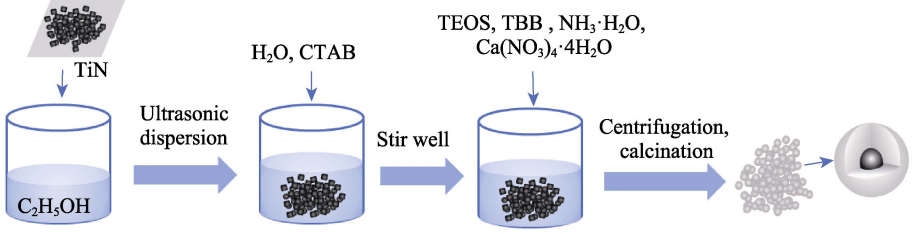

Fig. 1　Preparation process of core-shell *x*TiN@58S-20B nanoparticles

CTAB: Hexadecyl trimethyl ammonium bromide; TEOS: Tetraethyl orthosilicate; TBB: Tributyl borate

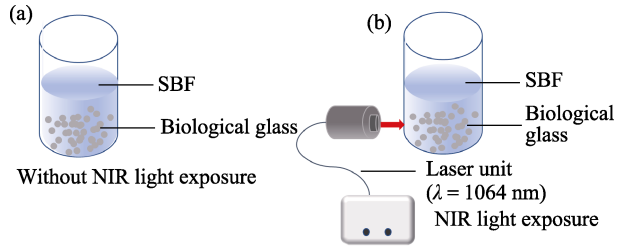

Fig. 2 Degradation of bioglass nanoparticles *in vitro* with and without laser irradiation

and shell layer (S_s) according to Eq. (1):

$$S = \pi r^2 \quad (1)$$

and the proportion of TiN NPs in the cross-section area (S_c/S_s). Similarly, the volume of nuclear layer and shell layer were calculated according to Eq. (2):

$$V = \frac{4}{3}\pi r^3 \quad (2)$$

and then their ratio (V_c/V_s) was obtained.

1.5 Photothermal performance

Photothermal properties of 58S-20B, 0.02TiN@58S-20B, and 0.04TiN@58S-20B were characterized under a 1064 nm NIR laser. 0.1 g of each of the three samples were taken to stack into a small cone with a bottom diameter of 1 cm, and the NIR laser with different power densities was irradiated at the samples at 25 ℃. The thermal images and temperature change were acquired using an infrared thermal camera.

1.6 Cell proliferation and cell morphology

The rBMCs were prepared cell suspension, inoculated into a 25 mL culture bottle, and placed in a 37 ℃, 5% CO_2 incubator. The medium was replaced every 3 d, and when the cells grew to 80%, trypsin (ThermoFisher, Shanghai, China) was added for digestion and passage, and the third-generation cells were selected for subsequent experiments. The glass particles (0.02 g) and 20 mL α-MEM (ThermoFisher, Shanghai, China) were added into the sterile centrifuge tubes, and the material extract was obtained after the tubes were placed in the incubator for 72 h.

The CCK-8 method was used to detect the effect of the soaking solution of each group of samples on cell proliferation[21-22]. Passage 3 of the cells were seeded at 96 well plates at a density of 5×10^4 mL^{-1}, 100 μL material extract was added into each well, and the well plate without extract was used as the control group. At given time points (3, 5, 7 d), the medium was eliminated and 10% CCK-8 was added to each well. After incubating in 5% CO_2 at 37 ℃ for 2 h, the samples were measured at 450 nm by a microplate reader.

To study the spreading and morphology of rBMCs at 3, 5, and 7 d, the cultured cells were washed three times with PBS and fixed in 4% paraformaldehyde (ThermoFisher, Shanghai, China) for 10 min and permeabilized with 0.1% TtitonX-100 solution in PBS for 5 min. TRITC-Phalloidin and 4′,6-diamidino-2-phenylindole (DAPI) diluted in 1% BSA were adopted to stain the cytoskeleton (red) and nuclei (blue). The staining results were captured using a confocal fluorescence microscope (SP8; Leica, Germany)

2 Results and discussion

2.1 Morphology and structure analysis

The borosilicate bioglass nanoparticles were uniform spherical particles with relatively uniform distribution (Fig. 3(a1)) of which the size of 58S-20B particles were among 550–650 nm. After TiN NPs were added, the glass spheres were fuller and the particle size increased (Fig. 3(b1-c1)) while the particle sizes of 0.02TiN@58S-20B and 0.04TiN@58S-20B were mainly distributed in 650–750 nm and 750–850 nm, respectively. After incorporation of TiN NPs, black matter appeared in the center of the glass particles obviously (Fig. 3(a2-c2)). With the increase of incorporation amount of TiN NPs, the volume proportion of black matter increased. The proportion of TiN NPs in the cross-section area elevated from 5% to 10% accompanied by volume ratio elevated from 1.2% to 3.5%, indicating the formation of core- shell structure of borosilicate bioglass. Their corresponding EDS spectra (Fig. 3(a3-c3)) confirmed that after TiN NPs being added, Ti and N were present in the 0.02TiN@58S-20B and 0.04TiN@58S-20B, and the more TiN NPs were added, the higher the element contents of Ti and N were.

Fig. 4 reveals the XRD patterns of the three samples. 58S-20B has no TiN NPs characteristic peaks, while these peaks appear in XRD patterns of 0.02TiN@58S-20B and 0.04TiN@58S-20B. Compared with the standard card PDF 09-0432, the diffraction peaks at 2θ=33.66°, 42.60°, and 61.81° corresponded to the (111), (200), and (220) crystal planes of TiN. The intensity of TiN's characteristic diffraction peak increased with the rising amount of TiN NPs. Moreover, the ratio of peak area to the "steamed bun peak" of glass also increased from 2% (B/b) to 4% (C/c).

Therefore, TiN NPs have been successfully incorporated into borosilicate bioglass particles to form a composite bioactive glass with TiN NPs as the core and borosilicate bioglass as the shell.

2.2 Photothermal performance

To evaluate the photothermal effect, 58S-20B, 0.02TiN@58S-20B, and 0.04TiN@58S-20B were irradiated by a 1064 nm NIR laser[23-24]. The temperature of 58S-20B nanoparticles was kept at about 25 ℃ under

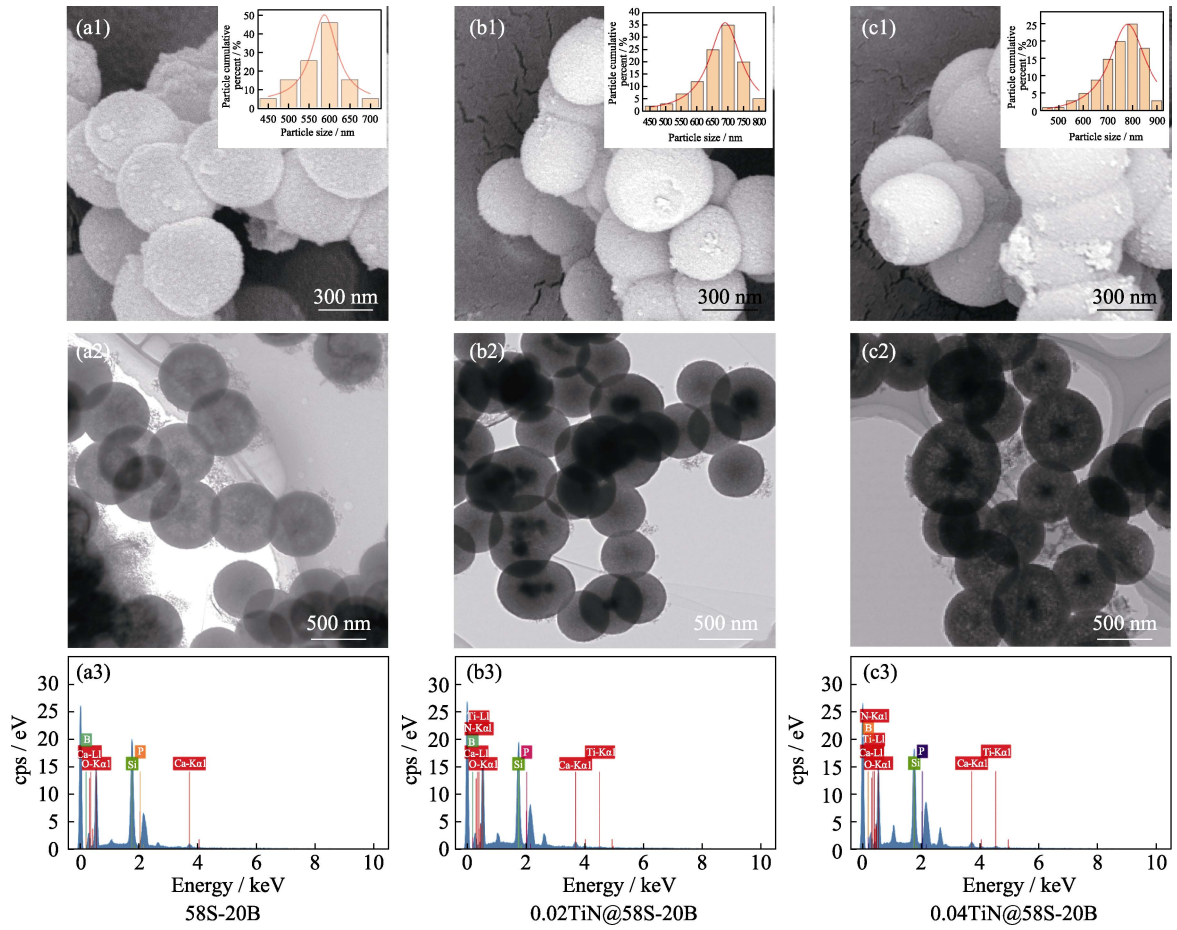

Fig. 3　Micrographs of *x*TiN@58S-20B (*x*=0, 0.02, 0.04) with insets showing the corresponding particle size distributions (a1, b1, c1) SEM images; (a2, b2, c2) TEM images; (a3, b3, c3) EDS spectra

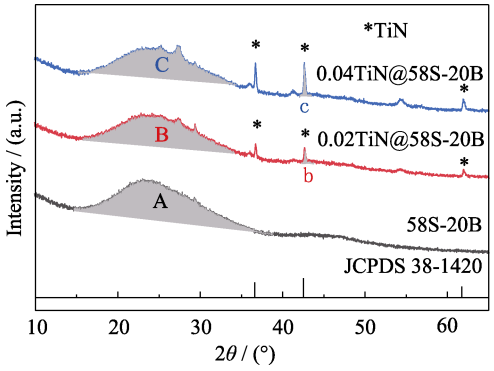

Fig. 4　XRD patterns of *x*TiN@58S-20B (*x*=0, 0.02, 0.04), with gray shaded parts A, B, and C showing the glass peak areas, while b and c showing the strongest peak area of the TiN NPs

laser irradiation and did not change with the extension of loading time, which meant there was no photothermal effect (Fig. 5(a1-a5)). In contrast, the bioglass doped with TiN NPs showed an obvious photothermal effect (Fig. 5 (b1-b5, c1-c5)). The temperature rise of core-shell microspheres both happened rapidly within 1 min, of which 0.02TiN@58S-20B raised from 25.0 ℃ to 60.4 ℃ while 0.04TiN@58S-20B raised to 96.3 ℃. What's more, the areas where temperature rose are controlled within a very small range, indicating that the temperature rise of the samples cannot affect the surrounding environment.

Influence of power density and TiN NPs content on sample temperature and stability of the sample photothermal effect (Fig. 6). For 58S-20B, the temperature did not change with the NIR laser irradiation (Fig. 6(a)), indicating no photothermal effect. For bioglass doped with TiN NPs, when power density is 0.38 W/cm^2, the optical energy of NIR laser cannot be converted into heat energy resulting in no temperature change (Fig. 6(b, c)); Fig. 6(d) reveals the minimum power requirements for a temperature rise of TiN NPs. With the increase of power density, the energy provided by 0.42 W/cm^2 exactly excited TiN NPs to undergo energy level transition. When the power density exceeded 0.42 W/cm^2 (Fig. 6(b, c)), the surface temperature of composite bioglass with different TiN NPs content increased with the extension of irradiation time. The higher the power density and the more doping concentration of TiN NPs, the stronger the heating effect is. The temperature of the sample rose rapidly in the first 10 s, reached saturation at 180 s after irradiation, and balanced generation- dissipation without change thereafter. These results demonstrated that TiN

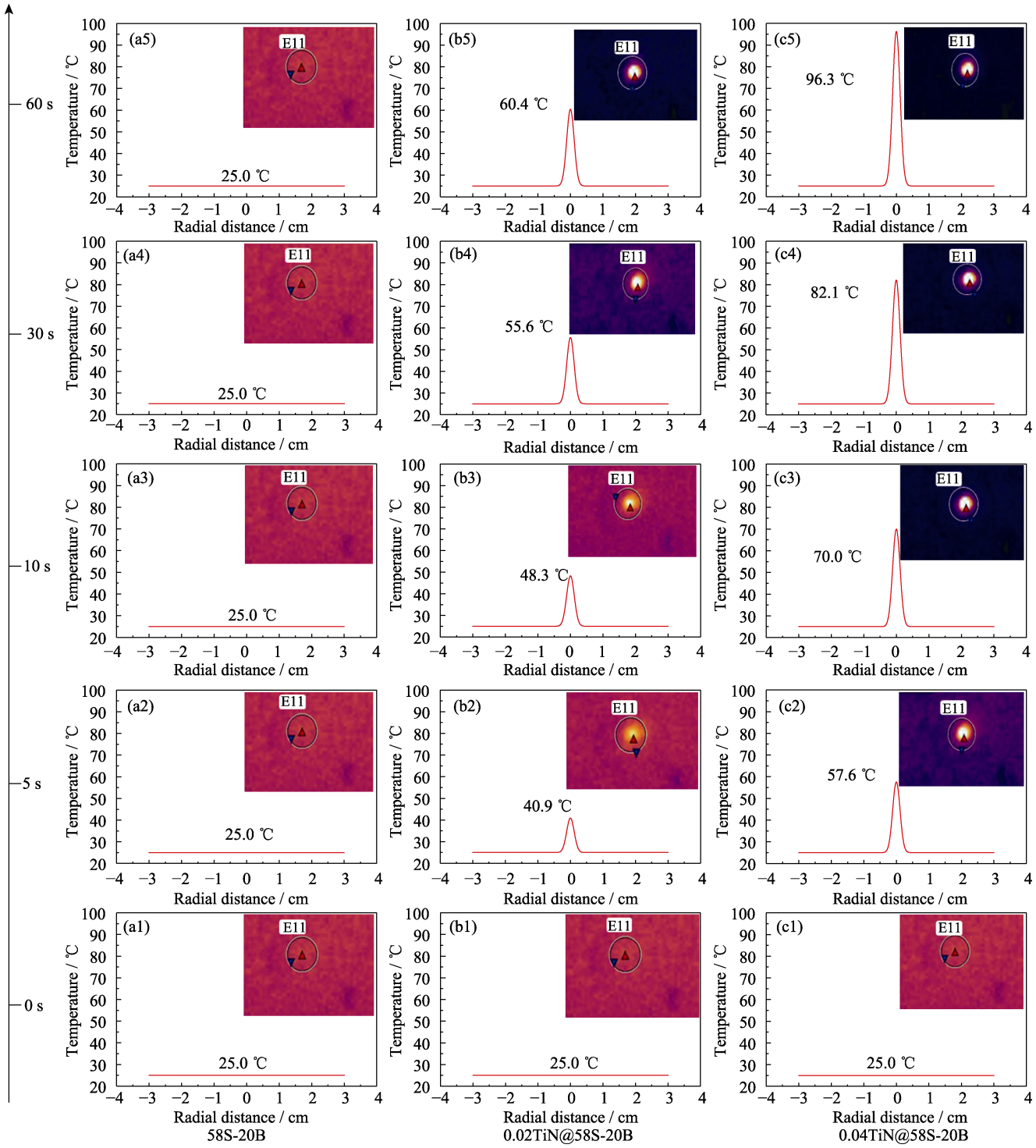

Fig. 5 Temperature rise diagrams of three samples in air with 1064 nm NIR laser at a power density of 1.0 W/cm^2 for 60 s, with insets showing the infrared images correspondingly at each time point, *X* axial representing the radial distance extending to both sides from the sample center, and the *Y* axial representing the temperature

NPs can efficiently convert laser's optical energy into heat energy.

To test the reliability and stability of the photothermal performance of the samples, 58S-20B, 0.02TiN@58S-20B, and 0.04TiN@58S-20B were subjected to 1064 nm NIR laser irradiation for several 3 min consecutive cycles. As shown in Fig. 6(e), in each heating-cooling process, the temperature change is closely dependent on whether the laser is loaded or not. That is to say, the temperature rose immediately as soon as the laser loaded, and the temperature dropped the moment the laser removed. In the three cycles, the heating period, cooling period and temperature change amplitude under the same power density are almost the same. In conclusion, the

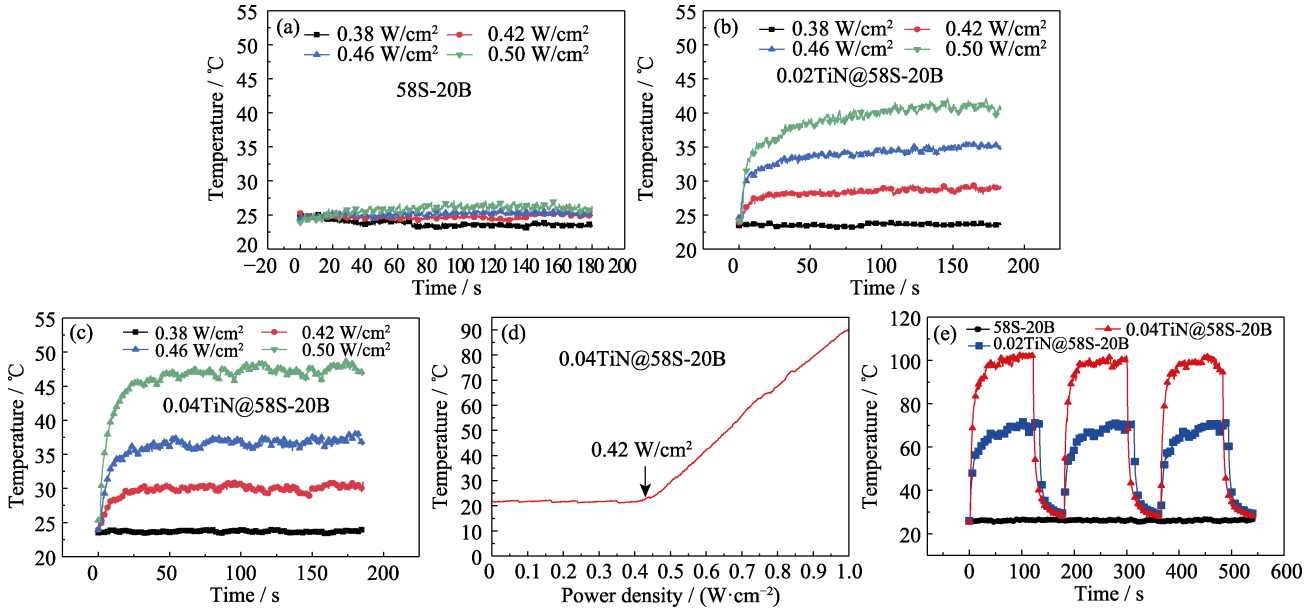

Fig. 6　Temperature changes of bioglass

(a-c) Temperature changes of 58S-20B (a), 0.02TiN@58S-20B (b), 0.04TiN@58S-20B (c) irradiated by 1064 nm NIR laser at different power density (0.38, 0.42, 0.46, 0.50 W/cm^2) for 3 min; (d)Temperature *versus* power density; (e) Heating curves of three samples under 1064 nm laser irradiation (1.0 W/cm^2)

core-shell bioglass microspheres have controllable and stable photothermal effects. It can withstand repeated laser irradiation for a long time. Therefore, the temperature of borosilicate bioglass can be effectively controlled by laser loading in photothermal bone therapy.

2.3　Degradation performance analysis

The biodegradability and biological activity could be reflected by the pH change of the immersion solution *in vitro*. To evaluate the effect of photothermal effect on the ion release ability and degradation ability of borosilicate bioglass, 58S-20B, 0.02TiN@58S-20B, and 0.04TiN@58S- 20B were immersed in SBF and irradiated with laser. As is shown in Fig. 7(a-c), during the degradation of the samples, pH of the soaking solution gradually rose and tended to be flat because the ions in the glass gradually dissolved and rapidly exchanged with the H^+ or H_3O^+in the body fluid[25]; After the infrared light irradiation, pH of the three samples soaking solutions showed different trends. The pH of 58S-20B remained almost unchanged, while the pH of 0.02TiN@58S-20, 0.04TiN@58S-20B increased significantly, with ranges from pH 8.06 to pH 8.27 and from pH 8.12 to pH 8.29, respectively, on the first day of soaking. This result indicates that photothermal can improve the biodegradability of TiN NPs doped borosilicate bioglass *in vitro*.

Above rise of pH is due to the difference in the acidity and alkalinity of the ions involved in the solution precipitation reaction during the conversion process, and Fig. 7(d-f) reveals the concentration of silicon, boron, and calcium from three samples with and without laser irradiation during 7-d dissolution. Without photothermal loading, the incorporation of TiN NPs contributed to the slight increases of the concentration of boron, silicon, and calcium in the solution. Since particle size of bioglass was gradually increased due to incorporation of the ions exchange between glass microspheres, the ion content in soaking solution of 0.02TiN@58S-20B was greatly changed. As the content of TiN NPs was further increased, the content of bioglass in each unit mass decreased, and the change of ions in soaking solution of 0.02TiN@58S-20B was weakened. After irradiation, the concentration of three ions changed a little in the 58S-20B immersion solution, but greatly changed in 0.02TiN@58S-20B and 0.04TiN@58S-20B immersion solution in which the concentration of boron and calcium was significantly increased because photothermal effect promoted the dissolution of calcium ions and boron ions. Calcium was increased by about 16% and 12%, respectively, and boron was increased by 11% and 8%, respectively. During the mineralization, condensation and repolymerization of Si–OH led to the formation of a SiO_2-rich layer on the glass surface depleted alkalis and boron ions[26]. The photothermal effect is conducive to formation of the SiO_2-rich layer, resulting in concentration of silicon to be reduced to a certain extent. It reveals that the NIR laser has a significant effect on the degradation process and the release rate of ions of TiN@58S-20B.

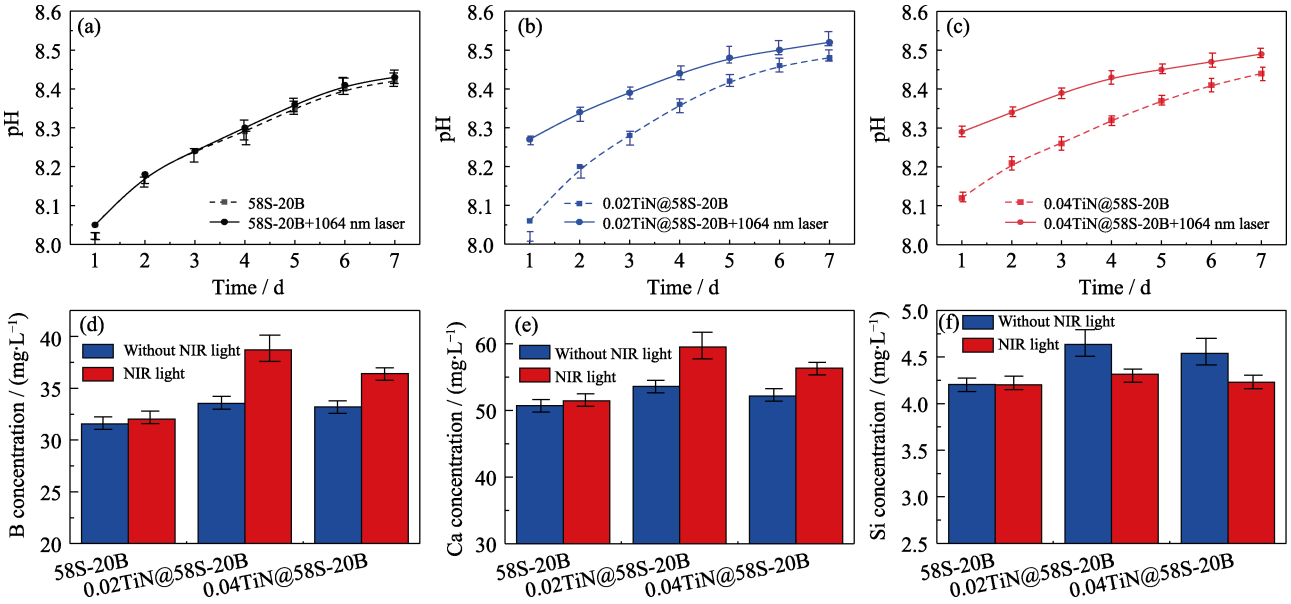

Fig. 7 pH changes and ions release of bioglass samples immersed in SBF at 37 ℃ for 7 d
(a-c) pH changes within 7 d; (d-f) Ion release profiles of B, Ca, Si on the 7th day

2.4 *In vitro* mineralization analysis

To evaluate the influence of the photothermal effect on the mineralization of three borosilicate bioglass, 58S-20B, 0.02TiN@58S-20B, and 0.04TiN@58S-20B were immersed in SBF and irradiated with or without a 1064 nm NIR laser for 7 d. Fig. 8 shows the microscopic morphology and energy spectrum analysis of bioglass nanoparticles after immersion. Micromorphologies of 58S-20B before and after laser loading shows almost no change (Fig. 8(a1-a2)). EDS analysis shows that Ca/P increased from 0.81 to 0.87 without significance, indicating light and heat have little effect on the mineralization of 58S-20B. In contrast, after laser loading, a large number of closely arranged agglomerated pellets forms on the surface of 0.02TiN@58S-20B and 0.04TiN@58S-20B. EDS results showed that Ca/P increased from 1.07 and 1.15 to 1.27 and 1.43, respectively, which was approaching 1.67, the calcium-phosphorus ratio of HA. These outcome reveals that the light and heat can promote the formation of mineralized products of 0.02TiN@58S-20B and 0.04TiN@58S-20B.

Fig. 9 reveals the XRD patterns of the mineralized products in the solution of the three samples soaked in SBF for 7 d. After immersion for 7 d, sharp diffraction

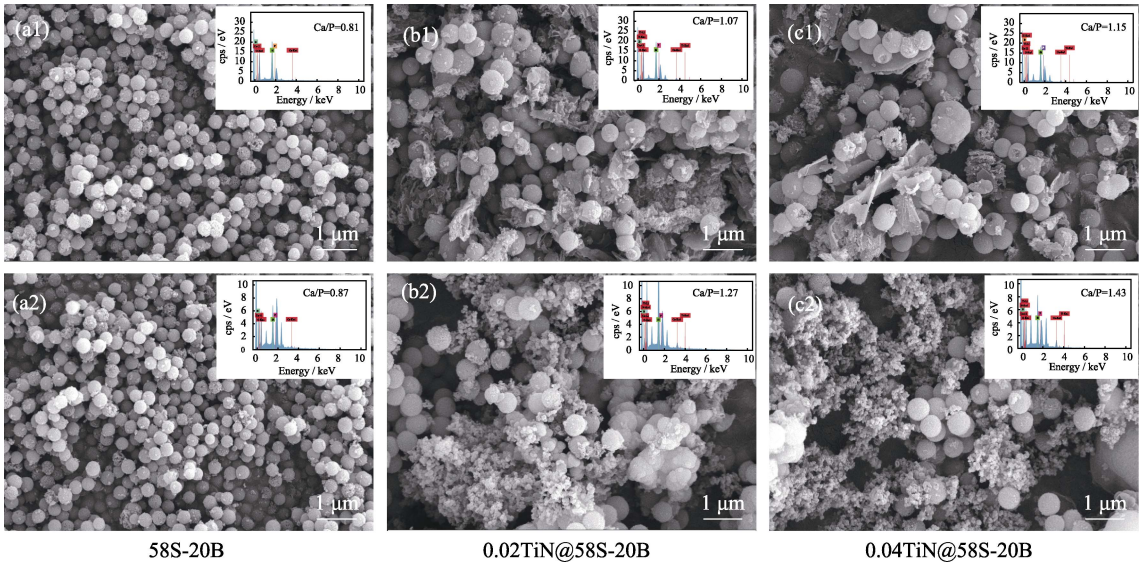

Fig. 8 SEM images of borosilicate samples immersed in SBF for 7 d with insets showing corresponding EDS spectra
(a1, b1, c1) Without NIR laser irradiation; (a2, b2, c2) With NIR laser irradiation

peaks begin to appear in the pattern. Compared with the standard card PDF 19-0272, the diffraction peaks at 2θ=25.73° and 32.17° correspond to the (002) and (112) crystal planes of hydroxyapatite $Ca_{10}(PO_4)_3(CO_3)_3(OH)_2$. After being photothermal irradiated, the intensity of the diffraction peak in the XRD patterns of 0.02TiN@58S-20B, and 0.04TiN@58S-20BTiN increased significantly, indicating that the NIR laser loading promoted the formation of mineralized products of the borosilicate bioglass doped with TiN NPs in the process of immersion *in vitro*.

2.5　Cell proliferation and morphology

To evaluate the effect of TiN@58S-20B on osteoblast activity and cell morphology, the cells was evaluated by CCK-8 staining after 3, 5 and 7 d of inoculation (Fig. 10(a)). The CCK-8 analysis of osteoblasts shows that compared with control group, osteoblasts cultured in the biological glass extract has higher activity, reflecting the role of biological glass in promoting cell proliferation. In addition, the osteoblast activity in the extracts of the three groups of samples is significantly improved, but for 0.02TiN@58S-20 and 0.04TiN@58S-20B, the improvement is slightly weak. However, it still has high activity, which indicates that the incorporation of TiN NPs has no significant side effect on the biocompatibility of bioglass.

The laser confocal photos of osteoblasts co-cultured with bioglass extracts for 7 d show that the three groups of cells are complete in morphology, in the shape of polygon of short fiber rotor, evenly distributed and well extended(Fig. 10(b)). Thus, the incorporation of TiN NPs does not affect the normal growth of cell morphology.

Therefore, the bioglass is of good biosafety, and the generation of mineralized products has increased significantly under the load of photothermal field. HA has good bone induction, which can promote the growth of osteoblasts in human body[27]. Therefore, it can promote the degradation and mineralization of bioglass through the loading of photothermal field, thus promoting the growth of osteoblasts.

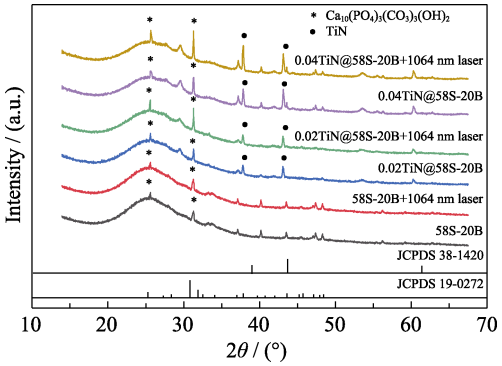

Fig. 9　XRD patterns of mineralization products of three samples with and without laser irradiation

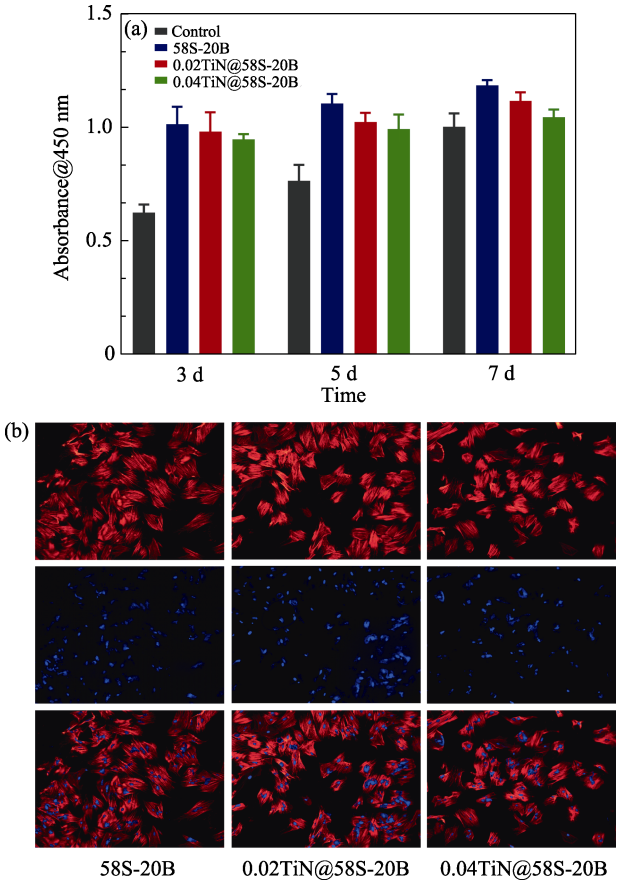

Fig. 10　Cell proliferation activity and cell morphology analysis of control, 58S-20B, 0.02TiN@58S-20B, and 0.04TiN@58S-20B
(a) CCK-8 analysis; (b) Fluorescent images of cell morphology. Blue indicates the cell nucleus and red indicates the cell cytoskeleton

3　Conclusions

The bioglass, with TiN NPs as core and borosilicate bioglass as the shell, can be prepared by Sol-Gel method. The results demonstrate that the nanoparticles show a significant photothermal effect, and the photothermal ability can be adjusted by regulating the amount of doped TiN NPs and power density. Under irradiation of a 1064 nm NIR laser, though, in the middle and late stage biological activity gradually declines, biodegradability and mineralization of bioglass can be improved through the regulation of the photothermal effect. The core-shell structure can concentrate the photothermal effect on the glass shell, which can significantly increase the temperature to accelerate the ion release and mineralization without damaging the cells. Thus, this work solved the problem of slow and uncontrollable rate in the middle and late stages of bioglass mineralization through *in vitro* photothermal regulation technology. *x*TiN@58S-20B, as a new type of core-shell structure multi-bioactive glass, provides a new idea for the application of photothermal field in bone repair.

References:

[1] DESCHASEAUX F, SENSÉBÉ L, HEYMANN D, *et al*. Mechanisms of bone repair and regeneration. *Trends in Molecular Medicine*, 2009, **15(9):** 417.

[2] BOSE S, ROY M, BANDYOPADHYAY A, *et al*. Recent advances in bone tissue engineering scaffolds. *Trends in Biotechnology*, 2012, **30(10):** 546.

[3] LARRY L, HENCH L L. Bioactive materials: the potential for tissue regeneration. *Journal of Biomedical Materials Research*, 1998, **41(4):** 511.

[4] KOKUBO T, ITO S, HUANG Z T, *et al.* Ca, P-rich layer formed on high-strength bioactive glass-ceramic A-W. *Journal of Biomedical Materials Research*, 1990, **24(3):** 331.

[5] HENCH L L, PASCHALL H A. Direct chemical bond of bioactive glass-ceramic materials to bone and muscle. *Journal of Biomedical Materials Research*, 1973, **7(3):** 25.

[6] SAEID K, FRANCESCO B, SEPIDEH H, *et al.* Bioactive glasses entering the mainstream. *Drug Discovery Today*, 2018, **23(10):** 1700.

[7] SAQIB A, IMRAN F, KEFI I, *et al.* A review of the effect of various ions on the properties and the clinical applications of novel bioactive glasses in medicine and dentistry. *Saudi Dental Journal*, 2014, **26(1):** 1.

[8] HU H R, TANG Y. Angiogenesis and full-thickness wound healing efficiency of a copper-doped borate bioactive glass/poly(lactic-co-glycolic acid) dressing loaded with vitamin E *in vivo* and *in vitro*. *ACS Applied Materials & Interfaces*, 2018, **10(27):** 22939.

[9] LI J, ZHANG C, GONG S, *et al.* A nanoscale photothermal agent based on a metal-organic coordination polymer as a drug-loading framework for effective combination therapy. *Acta Biomaterialia*, 2019, **94:** 435.

[10] ZHANG T, JIANG Z, XVE T, *et al.* One-pot synthesis of hollow PDA@DOX nanoparticles for ultrasound imaging and chemo-thermal therapy in breast cancer. *Nanoscale*, 2019, **11(45):**21759.

[11] CAO Z X, WANG R G, YANG F, *et al.* Photothermal healing of a glass fiber reinforced composite interface by gold nanoparticles. *RSC Advances*, 2015, **5(124):** 102167.

[12] PINHEIRO A N L B, SOARES L G P, DA SILVA A C P, *et al.* Laser/LED phototherapy on the repair of tibial fracture treated with wire osteosynthesis evaluated by Raman spectroscopy. *Lasers in Medical Science*, 2018, **33:** 1657.

[13] SMITH A M, MANCINI M C, NIE S, *et al*. Bioimaging: second window for *in vivo* imaging. *Nature Nanotechnology*, 2009, **4(11):** 710.

[14] JIANG W, FU Q, WEI H, *et al.* TiN nanoparticles: synthesis and application as near-infrared photothermal agents for cancer therapy. *Journal of Materials Science*, 2019, **54:** 5743.

[15] GULER U, SHALAEV V M, BOLTASSEVA A, *et al*. Nanoparticle plasmonics: going practical with transition metal nitrides. *Materials Today*, 2015, **18(4):** 227.

[16] ZHANG M, YAO A, LIN J, *et al.* Photothermally active borosilicate-based composite bone cement for near-infrared light controlled mineralisation. *Materials Technology*, 2021, **37(10):** 1243.

[17] ZHU K P, SUN J, SONG Y E, *et al.* A novel hollow hydroxyapatite microspheres/chitosan composite drug carrier for controlled release. *Journal of Inorganic Materials*, 2016, **31(4):** 434.

[18] LIANG Z, SUSHA A, CARUSO F, *et al*. Gold nanoparticle-based core-shell and hollow spheres and ordered assemblies thereof. *Chemistry of Materials*, 2003, **15(16):** 3176.

[19] KIM J, JI E L, LEE J, *et al.* Magnetic fluorescent delivery vehicle using uniform mesoporous silica spheres embedded with monodisperse magnetic and semiconductor nanocrystals. *Journal of the American Chemical Society*, 2006, **128(3):** 688.

[20] BALAS F, ARCOS D, PÉREZ-PARIENTE J, *et al.* Textural properties of SiO_2·CaO·P_2O_5 glasses prepared by the Sol-Gel method. *Journal of Materials Research*, 2001, **16(5):** 1345.

[21] SUN H Z, GE W J, GAO X, *et al.* Effect of SDT on the survival rate of endometrial cancer cells, assessed by the CCK-8 method. *PLOS ONE*, 2015, **11:** 27.

[22] GAO J, YE B, WU W H, *et al.* Tachyzoites of toxolasma gondii enhances the cytotoxicity of Etooside (V-16) to mouse colon cancer cell ct26 *in vitro*. *Chinese Journal of Zoonoses*, 2010, **26(8):** 720.

[23] JAQUE D, MAESTRO L M, ROSAL B D, *et al.* Nanoparticles for photothermal therapies. *Nanoscale*, 2014, **6(16):** 9494.

[24] MAESTRO L M, HARO-GONZÁLEZ P, ROSAL B D, *et al.* Heating efficiency of multi-walled carbon nanotubes in the first and second biological windows. *Nanoscale*, 2013, **5(17):** 7882.

[25] HENCH L L, WILSON J. Surface-active biomaterials. *Science*, 1984, **226(4675):** 630.

[26] YAO A H, LIN J, DUAN X, *et al.* Formation mechanism of multilayered structure on surface of bioactive borosilicate glass. *Chinese Journal of Inorganic Chemistry*, 2008, **24(7):** 1132.

[27] ZHU X, SCHEIDELER L, EIBL O, *et al.* Characterization of nano hydroxyapatite/collagen surfaces and cellular behaviors. *Journal of Biomedical Materials Research*, 2006, **1(14):**114.

光热核壳 TiN@硼硅酸盐生物玻璃纳米颗粒的降解和矿化性能

吴 锐[1], 张敏慧[1], 金成韵[1], 林 健[1,2], 王德平[1,2]

(同济大学 1. 材料科学与工程学院, 上海 201804; 2. 教育部土木工程先进材料重点实验室, 上海 200092)

摘 要: 硼硅酸盐生物玻璃以其稳定的结构和优异的生物活性而受到广泛关注, 但生物玻璃在矿化过程中活性呈现初期快而中后期慢的趋势, 造成后期的活性降低。光热可加速生物玻璃降解, 本研究制备了以氮化钛为核、生物玻璃($40SiO_2$-$20B_2O_3$-36CaO-$4P_2O_5$)为壳的复合生物玻璃, 利用光热场干预生物玻璃的矿化过程。结果表明, 生物玻璃具有显著的光热效应, 光热能力随氮化钛掺杂量和激光功率密度的增加而提高; 在体外浸泡中, 近红外光辐照促进了生物玻璃的降解, 浸泡 7 d 后模拟体液中钙、硼的含量分别增加 12%~16%和 8%~11%, 加速了羟基磷灰石的生成; 细胞增殖活性实验表明样品有良好的生物安全性。因此, 光热场可促进生物玻璃降解和矿化, 对周围细胞影响小, 有望在保障初期生物安全的同时发挥调节作用。

关 键 词: 硼硅酸盐生物活性玻璃; 核壳结构; 光热性能; 矿化性能

中图分类号: TQ171 **文献标志码:** A